Journal of *Marine Science and Engineering*

MDPI

Article

Multifactorial Controls on the Dongdaobei Submarine Canyon System, Xisha Sea, South China Sea

Meijing Sun [1,*], Hongjun Chen [1], Chupeng Yang [1], Xiaosan Hu [1] and Jie Liu [2]

[1] Key Laboratory of Marine Mineral Resources, Ministry of Natural Resources, Guangzhou Marine Geological Survey, Guangzhou 511458, China
[2] Key Laboratory of Gas Hydrate, Guangzhou Institute of Energy Conversion, Chinese Academy of Sciences, Guangzhou 510640, China
* Correspondence: sunmeijing0411@163.com

Abstract: The submarine canyons system is the most widely distributed geomorphic unit on the global continental margin. It is an important concept in the field of deep-water sedimentation and geohazards. Based on high-resolution multibeam bathymetry and two-dimensional seismic data, the dendritic canyon system north of Dongdao island is studied at the eastern Xisha area of the South China Sea. The Dongdaobei submarine canyon is distributed in water depths between 1000 and 3150 m. The main source area in the upper course of the canyon originates from the northwest of Dongdao platform and the Yongxing platform. The sediments from the source area are transported to the main canyon in the form of various gravity flows. Landslides on the slope significantly impact canyon evolution by delivering sediment to the canyon head and causing channel deflection through substrate failure and flow-path reorganization. A large number of pockmarks are distributed around the north slope of the main canyon. The small-scale channels, which are formed as a result of the continuous erosion of the pockmark chains, are connected to the canyon sidewalls. The seamounts are distributed along the south bank of the canyon, exerting a controlling influence on the directional changes in the main canyon's downstream segment. The formation and evolution of the Dongdaobei submarine canyon are primarily influenced by several factors, including tectonic activity and inherited negative topography, erosion by sedimentary gravity flows, sediment instability, and the shielding effect of seamounts.

Keywords: canyon system; topography; configuration; Xisha sea area; South China Sea

check for updates

Academic Editors: Manuel Martín-Martín, Qiliang Sun, Chaoqi Zhu and Kiichiro Kawamura

Received: 29 November 2024
Revised: 5 March 2025
Accepted: 6 March 2025
Published: 14 March 2025

Citation: Sun, M.; Chen, H.; Yang, C.; Hu, X.; Liu, J. Multifactorial Controls on the Dongdaobei Submarine Canyon System, Xisha Sea, South China Sea. *J. Mar. Sci. Eng.* **2025**, *13*, 564. https://doi.org/10.3390/jmse13030564

Copyright: © 2025 by the authors. Licensee MDPI, Basel, Switzerland. This article is an open access article distributed under the terms and conditions of the Creative Commons Attribution (CC BY) license (https://creativecommons.org/licenses/by/4.0/).

1. Introduction

Submarine canyons frequently act as crucial pathways for terrigenous clastic sediments transported from the shelf to the abyssal plain [1–3]. Submarine canyons can also serve as pathways for the transport of clastic sediments from the carbonate platform slope to the deep sea. Most studies relating to submarine canyons have focused on the "source-sink" systems of siliciclastic depositional environments, whereas modern submarine canyons in carbonate settings have received less documentation [4–6].

The channel-fill complexes and depositional lobe systems outside the canyon mouth constitute favorable hydrocarbon reservoir targets [7–9]. These features have emerged as focal points in contemporary deepwater petroleum exploration studies [10,11]. These canyon systems are also active geological disaster areas, threatening the stability of projects such as the laying of marine cables [12,13], oil and gas pipelines, and the construction of drilling platforms. Therefore, ensuring the safety of marine engineering construction

areas has become an important research topic [14]. Tectonic activities affect the canyon depositional system [15,16]. Active faults can cause differential subsidence within the depositional strata, changing the topography from the platform margin slope to the abyssal area, and thereby affecting the development and distribution of gravity flow deposits.

The Dongdaobei submarine canyon, as a deep-water modern submarine canyon developed in carbonate settings in the Xisha region, originated from the water area between Yongxing platform and Dongdao platform. Research on modern submarine canyons in the carbonate settings of the Xisha Sea area is relatively scarce. Existing studies have primarily focused on the morphology and sedimentary filling characteristics of these canyons [17–19]. Large amounts of carbonate sediment and/or siliciclastic materials are delivered into the Northwest Sub-Basin through different transport processes [19]. Transport processes from platform-top to adjacent slopes can trigger large-scale sediment destabilization features like mass transport deposits (MTDs) and gravitational collapses [17,18].

The depositional structure, processes, and tectonic control of the northern canyon system associated with Dongdao platform remain poorly understood. Therefore, we present the first detailed depiction of Dongdao submarine canyon in the eastern Xisha Island area, using high-resolution multibeam bathymetric and seismic data. The main objectives are as follows: to (1) quantitatively analyze the geomorphic characteristics of the submarine canyons and describe the canyon depositional structure characteristics, and to (2) discuss the impact of factors such as topography, tectonic activity, and sedimentary processes on the formation of submarine canyons. The study contributes to understanding the role of canyons in transporting sediments to adjacent deep-sea basins in carbonate platform environments.

2. Overview of the Study Area

2.1. Geological Background

The South China Sea, as the largest marginal sea in the western Pacific, experienced multiple episodes of seafloor spreading from the Late Cretaceous to the Early Miocene [20–23]. The Xisha Sea Area is bound by the Northwest Sub-basin (NWSB) to the east, Zhongsha platform to the south, and Central canyon to the north. The tectonic evolution of the Xisha Sea Area can be divided into two stages [23–25]. During the early Cenozoic rift stage, the Xisha Sea Area experienced intense fault activity, forming a series of NE-trending and NW-trending faults [26]. The pre-Cenozoic basement structure was uplifted to form an exposed topographic high [21,27,28]. From the Late Oligocene to the Early Miocene, seawater gradually submerged the Xisha uplift, which remained in a relatively stable thermal subsidence stage.

Since the Early Miocene, carbonate platforms and coral reefs have started to develop on topographic highs in the Xisha Sea Area [29,30]. The study area is located within the Xisha Sea Area, where numerous seamounts are distributed on the seabed (Figure 1) [31]. Volcanic activities are concentrated in two periods—the Pliocene and the Quaternary [24]. Large-scale submarine canyons, contour currents, and submarine landslides are well developed. Various sediments formed by bottom current processes have been identified in the deep-sea plain of the Xisha Sea, where the water depth ranges from 1000 to 1400 m [18].

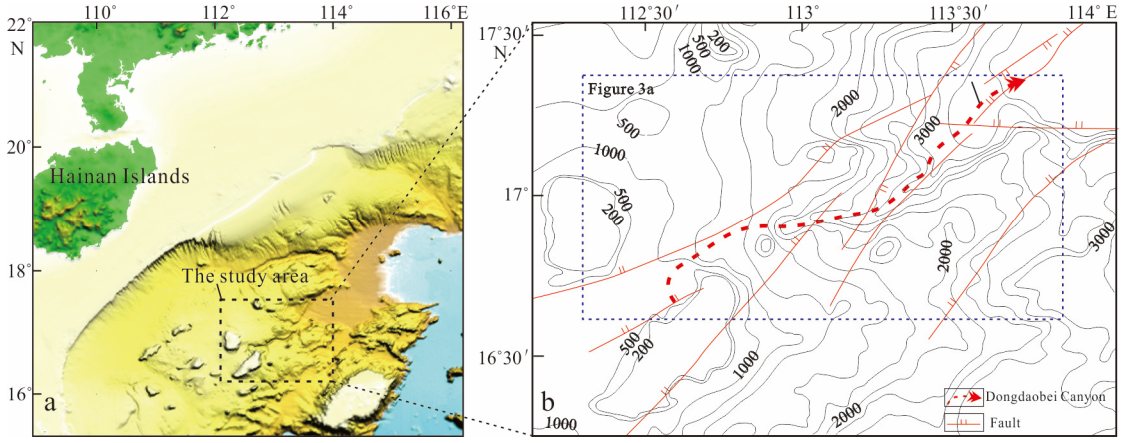


Figure 1. (**a**) Location of the research area. (**b**) Water depth and fault distribution in the eastern sea area of the Xisha Islands.

2.2. Stratigraphic Framework

The seismic interpretation in this study primarily focused on the analysis of seismic reflection characteristics, including amplitude, frequency, and continuity variations, as well as stratigraphic termination patterns such as truncation, onlap, and downlap relationships. This information was combined with regional drilling data and previous knowledge to classify the seismic strata in the study area (Figure 2) [24,32,33]. Well Xike 1 and Well Xiyong 1 were both drilled through the carbonate stratum of the Lower Miocene to depths of 1200 m. These wells revealed the Precambrian metamorphic bedrock and the Mesozoic igneous basement [34]. Five seismic reflection interfaces from the Neogene to the Quaternary were continuously tracked in this area (Figure 2). Of these interfaces, interface T_6 corresponds to the bottom interface of the Miocene, interface T_5 is the interface between the Middle and the Lower Miocene, interface T_3 is the interface between the Upper and the Middle Miocene, interface T_2 corresponds to the bottom interface of the Pliocene, and interface T_1 is the bottom interface of the Quaternary system.

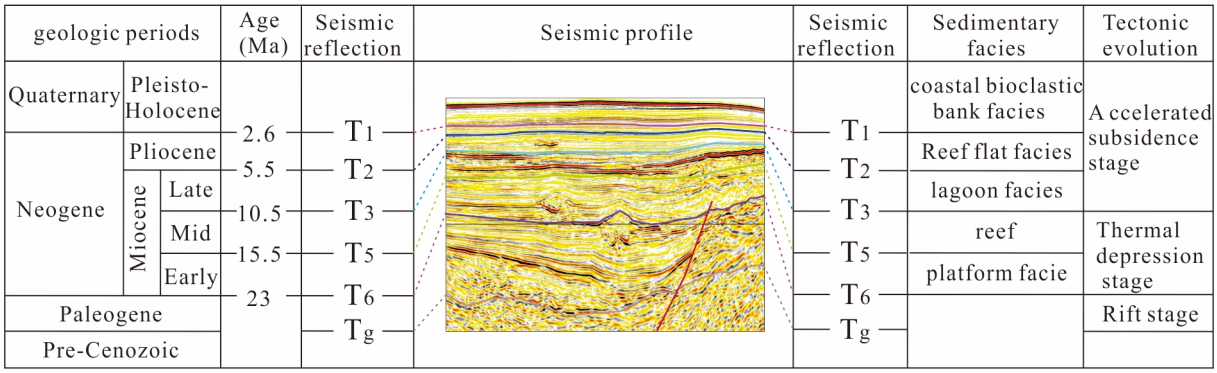


Figure 2. Seismic stratigraphic division of Xisha Sea Area.

3. Data and Methods

The multibeam bathymetric data, high-resolution single-channel seismic profiles, and multi-channel seismic profiles from the Guangzhou Marine Geological Survey were used in the study area. The SeaBeam2112 multibeam acquisition system (manufactured by L3Harris Technologies, Melbourne, FL, USA) was employed for water depth measurements, achieving a measurement accuracy of better than 0.5%. Bathymetric grid data were generated after applying a full-depth sound velocity profile correction using the Caris HIPS (v11.4) bathymetric data processing software. The grid data processing workflow incorporated

system parameter correction, ship attitude correction, and other post-processing procedures. Subsequently, the Global Mapper (v17) software was then used to plot bathymetry maps and three-dimensional topographic maps.

Single-channel seismic data were typically acquired at a boat speed of 4 to 6 knots. The acquisition system utilized an electric sparker source with a maximum energy of 10 kJ, providing a vertical resolution of 5 to 10 m. Data processing was conducted using the CGG-Geocluster (v3100) software, implementing standard processing procedures including amplitude recovery, surge static correction, and multiple wave suppression. For multi-channel seismic acquisition, the source capacity was 3810 cu.in., with a channel interval of 12.5 m and 480 active channels. The acquisition parameters included a sampling rate of 2 ms and a record length of 12 s. The processing workflow incorporated early-stage processing, velocity analysis, and multiple wave suppression, which effectively enhanced data quality by suppressing multiples and improving the signal-to-noise ratio. Both single- and multi-channel seismic data were interpreted using the Geoframe software (v4.4).

4. Results

4.1. Morphological Features of Submarine Canyons

The Dongdaobei submarine Canyon is distributed across the eastern continental slope of the Xisha Sea Area. It originates from the north side of Dongdao Island of the Xisha Sea Area and extends northeastward, eventually merging into the Northwest Sub-basin (Figures 3a–c and 4a). The total length of the Dongdaobei canyon exceeds 137 km and the water depth ranges from 988 m to 3146 m (Figure 3c).

The canyon head is located on the northwest slope of the Dongdao platform. It consists of four branched canyons. These branched canyons converge into the main canyon at a water depth of 1500 m (Figure 3a). The area containing the branch canyons is designated as Area I (Figure 4a,b) and covers an area of 250 km^2. The branched canyons C1 and C2 exhibit a north–south trend, while C3 and C4 trend northwestward (Figure 4a). These four dendritic canyon systems converge into the main canyon, which maintains a north–northeast (NNE) orientation throughout its course. The transverse profiles of the four branched canyons display V-shaped morphologies. The maximum incision depths of the four canyons (C1, C2, C3, and C4) are 236 m, 263 m, 286 m, and 272 m, respectively (Table 1).

Based on the orientation and geomorphological characteristics of each segment, the main canyon was divided into four segments—A, B, C, and D (Figure 3b). Segment A, situated in the upper reaches of the main canyon, exhibits a predominantly west–east orientation with a measured longitudinal extent of 27.4 km. Incision depths within this segment range from 424 m to 544 m. Segment B, located in the upper part of the mid-reaches of the canyon, extends northeastward (NE) over a length of 32 km. This segment is characterized by a relatively straight morphology and displays a maximum incision depth of 403 m. Segment C is positioned within the lower part of the mid-reaches of the canyon and extends in a south–southeast (SSE) direction, with a total length of approximately 12 km. The incision depth of this segment is 349 m. Segment D represents the downstream section of the canyon and extends northeastward (NE) over a total length of 39.5 km. The maximum incision depth of this segment reaches 291 m. The terminus of Segment D is the canyon mouth, which has an incision depth of 70 m (Table 1). From the upper reaches to the lower reaches of the canyon, the incision depth generally decreases, while the width increases, resulting in an increasing width-to-depth ratio.

The Dongdaobei submarine canyon system displays marked contrasts in cross-sectional geometry. Segments A to C feature steep, V-shaped profiles with asymmetric sidewalls, where the northern slope measures 15–16°, in contrast to the gentler southern slope of 8–10° (Figures 4a and 5b,c). The lower part of Segment D transitions to a broad,

U-shaped morphology (Figure 5d). The slopes of the canyon sidewalls further diminish to less than 5° at the canyon mouth (Figure 5e). The submarine canyon system exhibits a progressive downstream attenuation of thalweg gradients (Figure 3c). The slope of the bottom of the canyon in Segments A, B-C, and D is 1.2°, 0.8°, and 0.6°, respectively. Multiple knickpoints are discernible within the slope gradient profile, with their locations coinciding precisely with the bends in the canyon (Figure 3c).

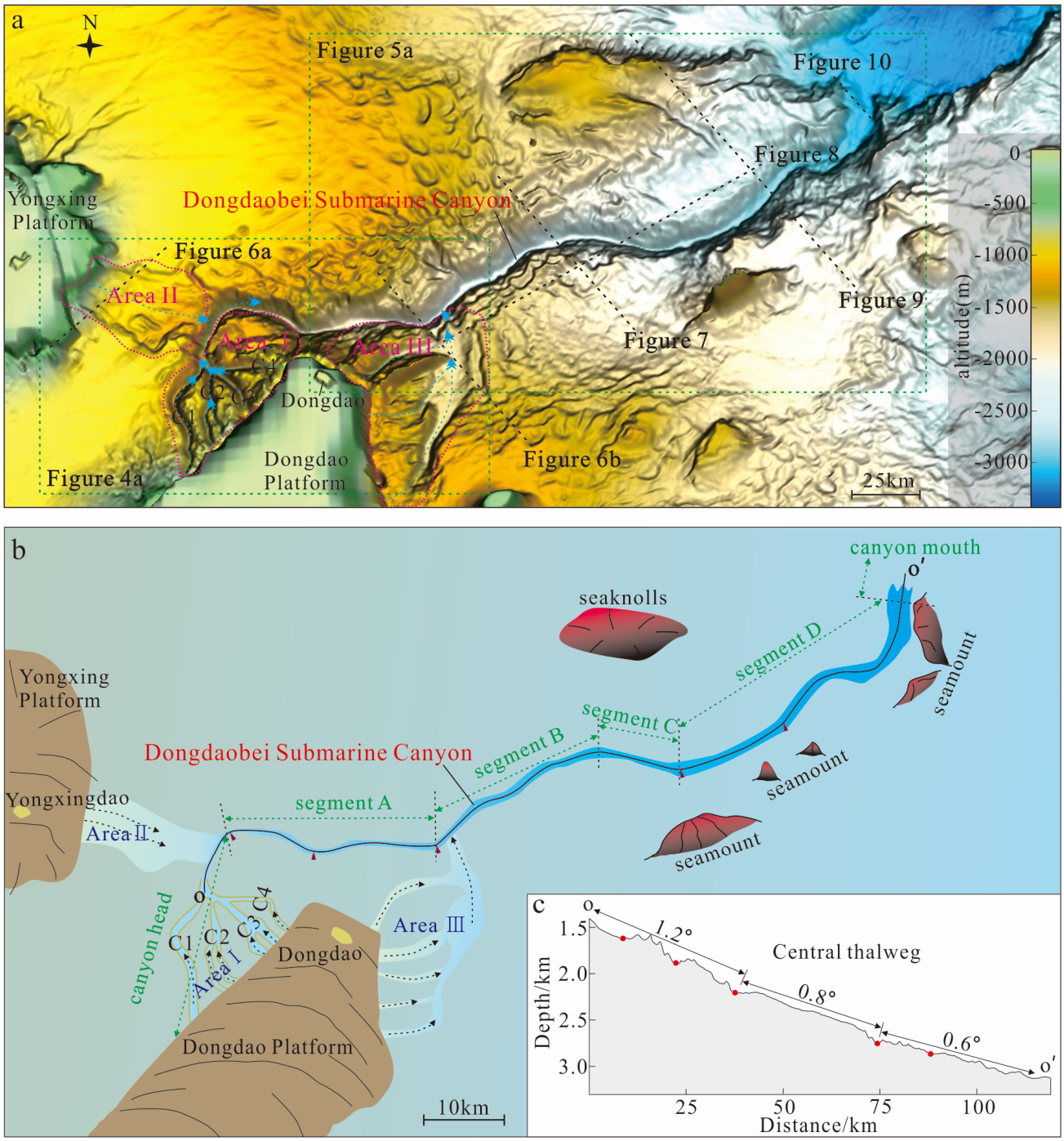


Figure 3. (**a**) Three−dimensional topographic map of the Dongdaobei submarine canyon (see Figure 1b for location). (**b**) Sketch of the plane distribution, division of the canyon segment, and location of the topographic profile of the canyon. (**c**) Topographic profile along the thalweg, with the red points indicating knickpoints (see Figure 3b for the profile location).

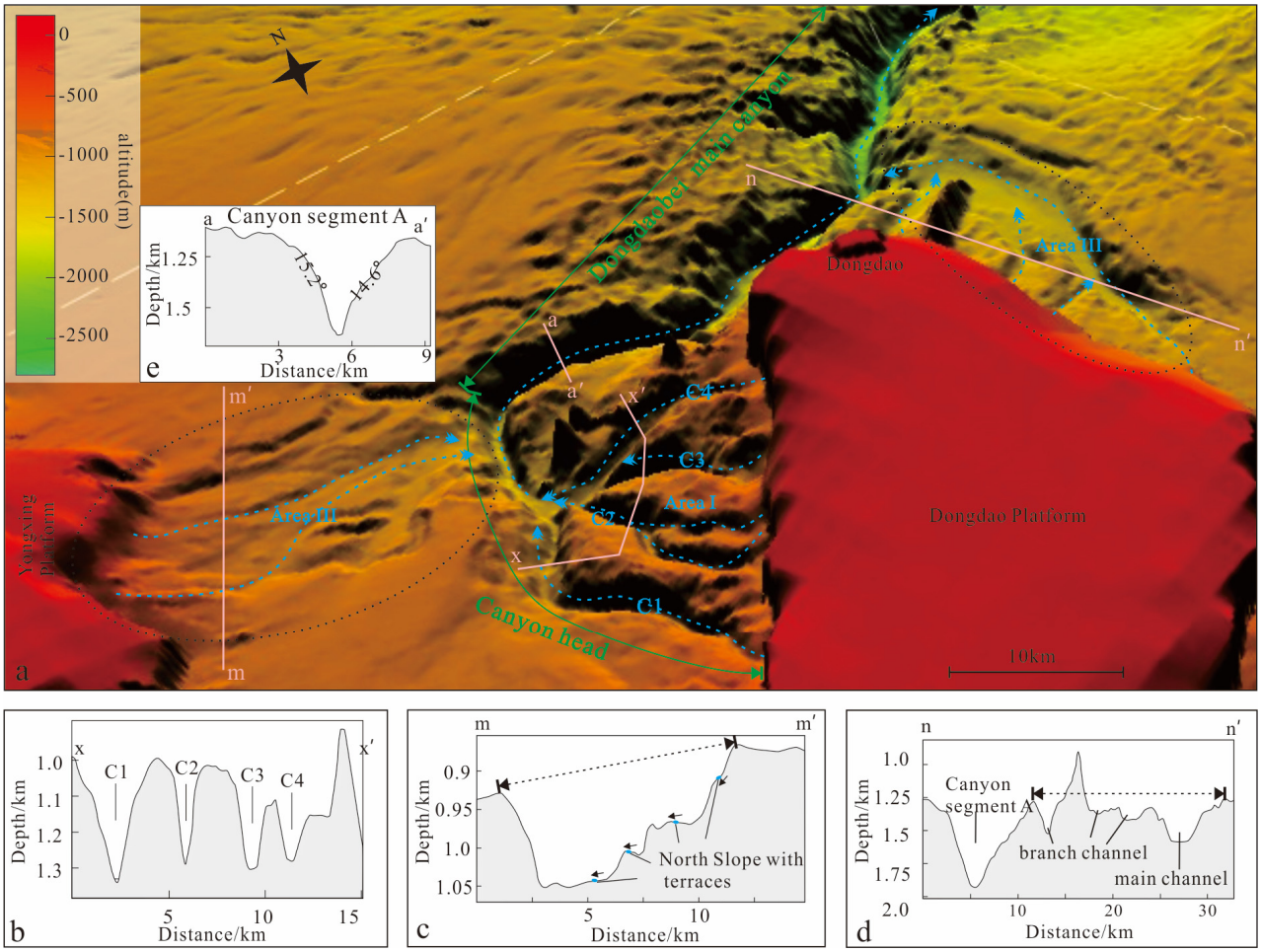


Figure 4. (**a**) Three−dimensional topographic map of canyon head and provenance area (see Figure 3b for location). (**b**–**e**) Topographic profile of canyon (see Figure 4a for the profile location).

Table 1. Summary of morphological parameters of Dongdaobei submarine canyon.

Canyon Segment		Strike	Water Depth (m)	Incised Valley Shape	Down Cutting Depth (m)	Top Section Width (m)	Breadth Depth Ratio	Recognizable Filling Thickness (m)
Canyon head	C1	N-NNW-NS	1187	V-shaped	236	2109	8.9	Unable to identify due to data limitations
	C2	NS	1239		263	2632	10	
	C3	N-NW	1262		286	2458	8.6	
	C4	N-NWW	1211		272	2664	9.8	
Canyon trunk	A	E	1574~2200	V-shaped	min 424	4879	11.5	
					max 544	4478	8.2	
	B	NE	2200~2399		min 453	3812	8.4	
					max 646	7879	12.2	
	C	E	2399~2704		min 367	7420	20.2	
					max 530	6400	12	
	D	NE-N	2704~3102	U-shaped	min 170	5071	29.8	45
					max 396	7533	19	

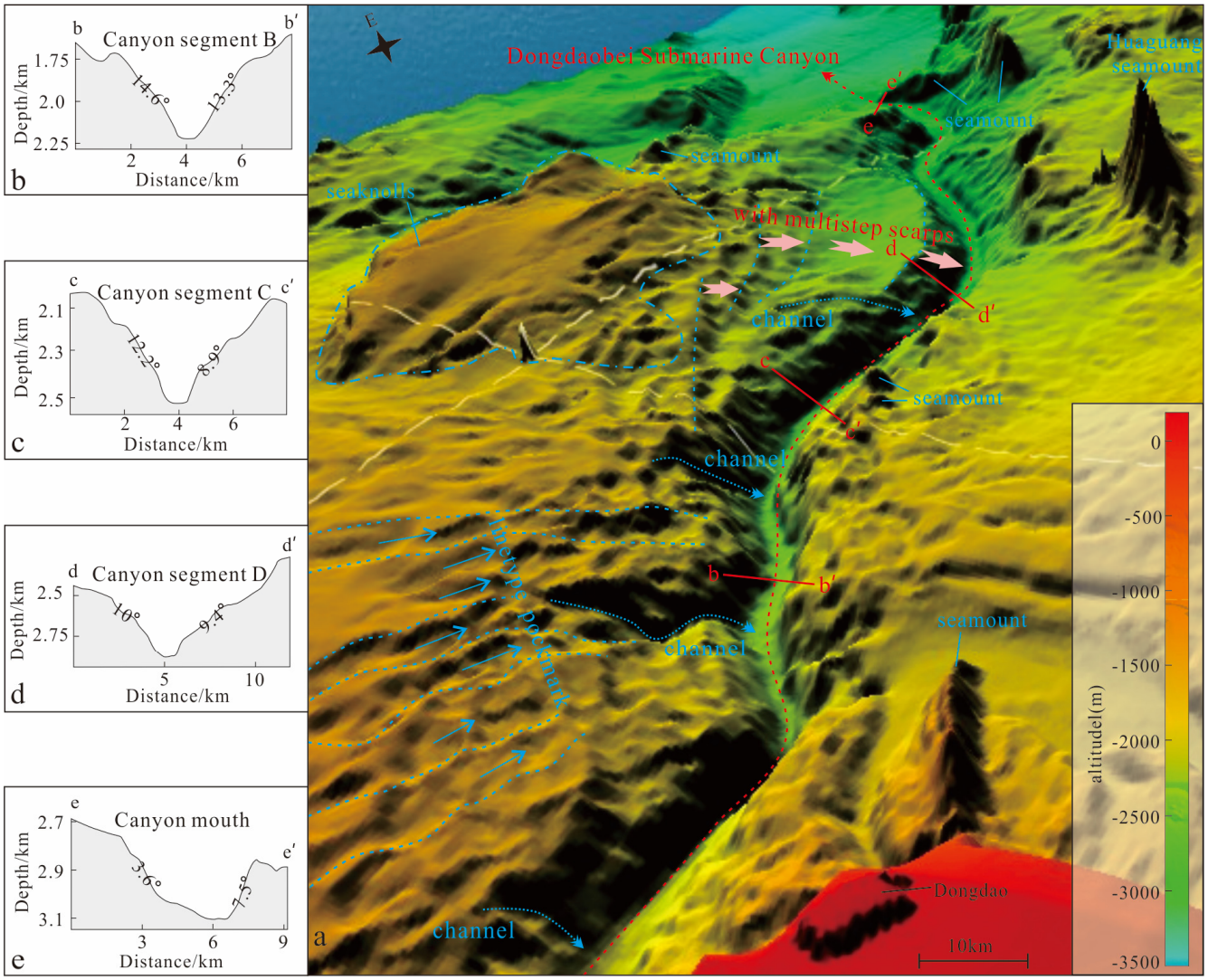


Figure 5. (**a**) Three−dimensional map showing the topographic features of the main canyon and both banks (see Figure 3a for location). (**b**–**e**) Topographic profile of canyon (see Figure 5a for the profile location).

The eastern slope area of the Yongxing platform scours down to form a channel group (Figure 4a), of which the water depth ranges from 564 to 1436 m. This area, labelled as the Area II channel group, is located on the northwest side of the upper segment of the canyon and covers an area of approximately 160 km^2, with a maximum incision depth of 188 m. This is shallower than the erosion depth of the branched canyon in Area I. Area II is characterized by extensive seafloor scouring, forming a prominent negative relief morphology interpreted as large-scale landslides (Figure 4a,c). The landslides exhibit a horseshoe-shaped morphology in plane view and concave profiles in the cross-section. They extend west–southwest from the Yongxing Platform to the canyon head, with steep gradients defining their headwalls and lateral margins (Figures 4b and 6a). A series of scarps and immature channels have developed within the landslides.

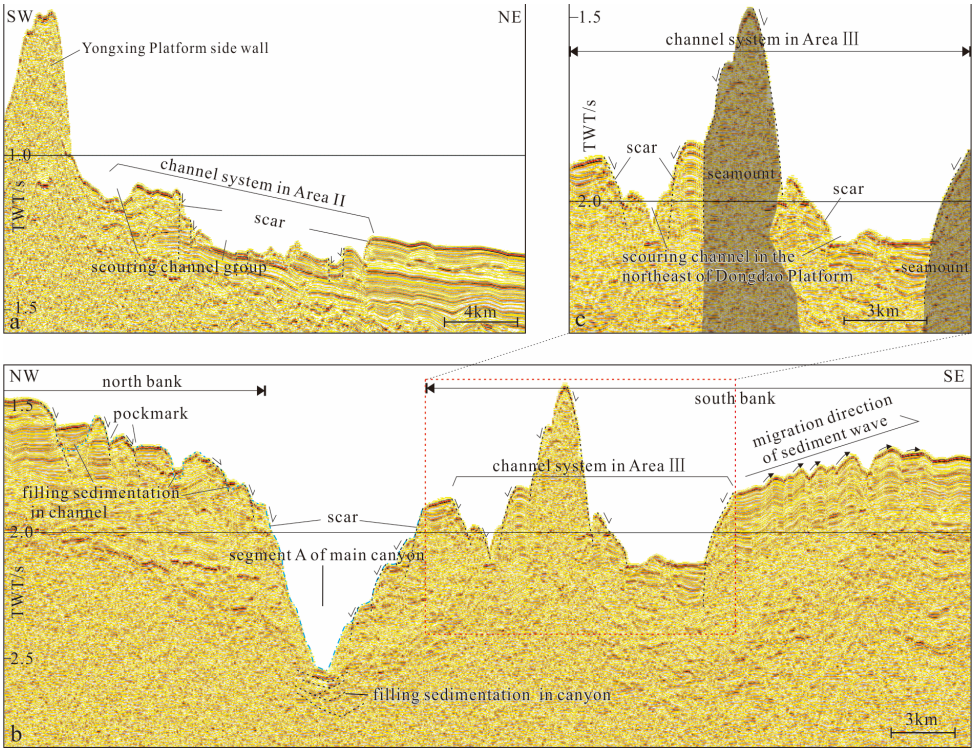


Figure 6. (**a**) Channel system of Area II shown by seismic profile. (**b**) Seismic profile through the channel system of Area III and the canyon. (**c**) Local enlarged interpretation of seismic profile (**b**) (see Figure 3a for profile location).

The northeastern side of the Dongdao platform is characterized by a group of eroded channels, referred to as the Area III channel group (Figure 4a,d). These channels, located at water depths of 1163–1662 m, consist of multiple northeast-trending branches that converge into a larger NNE-oriented channel. The NNE-oriented channel widens progressively from the southern upper reaches to the northern lower reaches, with widths ranging from 1.8 to 6 km and incision depths varying between 67 and 256 m. The channel ultimately connects to the initiation point of Segment B of the Dongdaobei canyon. The Area III channel group covers a total area of 225 km^2.

The topographic relief on the north bank of the canyon is higher than that on the south bank. The water depth on the north bank ranges from 1060 to 3000 m, while that on the south bank varies between 1140 and 3120 m. The slope of the north bank is 1° to 3° steeper than that of the south bank. Canyon Segments A–C cumulatively span approximately 65 km, with their northern flank exhibiting dense clusters of submarine pockmarks and erosional channels covering an area exceeding 1000 km^2 (Figures 3a and 5a). Detailed morphological analysis reveals distinct spatial variations in pockmark characteristics along the northern canyon margin. Within proximal zones (<7.5 km from the northern canyon bank), pockmarks exhibit significant overlap and clustering, resulting in complex superimposed morphologies. In contrast, distal regions display well-defined individual pockmarks with clearer morphological expression. Individual pockmarks predominantly exhibit two characteristic forms—crescent-shaped features and quasi-elliptical structures. Notably, the long axes of both pockmark types show preferential NW-SE alignment, systematically oriented toward the central thalweg of the main canyon.

4.2. Depositional Architecture of the Canyon

4.2.1. Sediment Provenance Systems

Located at the head of Dongdaobei canyon, Area I constitutes the primary sediment source for the canyon system (Figures 4a and 6a). Dendritic tributaries with deeply incised V-shaped profiles (width: 2.1–2.6 km; incision depth: 230–280 m) directly connect to the Dongdaobei canyon. These channels efficiently transport carbonate detritus from the northwestern margin of the Dongdao platform, exhibiting seismic reflections characterized by high amplitude and moderate-to-low continuity, with sediment accumulation thickness reaching approximately 50 m.

The Area II channel group delivers carbonate debris from the eastern Yongxing Platform to the upstream boundary of Segment A. Prolonged erosion has amalgamated individual channels into a contiguous incised valley (top width: ~10 km). Seismic profiles reveal limited deposition within the valley floor, with only scattered seabed remnant blocks preserved (Figure 6a). Slump deposits dominate this slope-unstable region, characterized by chaotic seismic reflections that obscure the original channel boundaries. These deposits are particularly prominent near the platform margin, where they form extensive accumulations with disordered internal structures.

The Area III channel group transports carbonate debris from the northeastern margin of the Dongdao platform to the middle reaches of Dongdaobei canyon. Seamounts and seahills in Area III separate the channels in this area (Figure 6b,c). The channel starts on the northeastern slope of the Dongdao island platform and extends for 6–14 km to converge on an NNE-trending main channel. The carbonate debris carried by the main channel then converges into Segment B of the canyon. Seismic reflections display medium amplitude with medium–low continuity and two-way onlap terminations. A 10-m-thick sedimentary fill is identified beneath the channel floor (Figure 5c).

4.2.2. The Sedimentary Filling of the Main Canyon

The seismic profile reveals that the main sedimentary fill thickness of the Dongdaobei canyon generally ranges from 50 to 80 m. The cross-sectional morphology of Segments A, B, and C in the Dongdaobei canyon is characterized by a V-shaped profile (Figures 6b, 7, 8a–c and 9), while Segment D exhibits a U-shaped cross-sectional configuration. The submarine filling thickness of Segment A in the main canyon was about 16 m (Figure 6b), and multiple stages of depositional filling occurred. The bottom interface of the canyon in each stage extruded to the deep parts, showing a strong amplitude and continuous reflection. There is medium continuous or scattered reflection filling in the canyon. Landslides occurred on the side walls of the canyon, and the submarine filling depth of Segment D in the canyon is about 45 m. Two stages of depositional filling have developed under the seafloor since the Middle Miocene. There is a clear reflection boundary between the canyon's bottom and its deposits. The first stage of filling in the lower part of the canyon shows strong amplitude, medium continuity, and sub-parallel structure reflection. The second stage of filling in the upper part is close to the seafloor and is characterized by a chaotic structure and irregular shape. The deposits on the side walls of the canyon migrated to the canyon bottom via landslides and were deposited on the canyon floor.

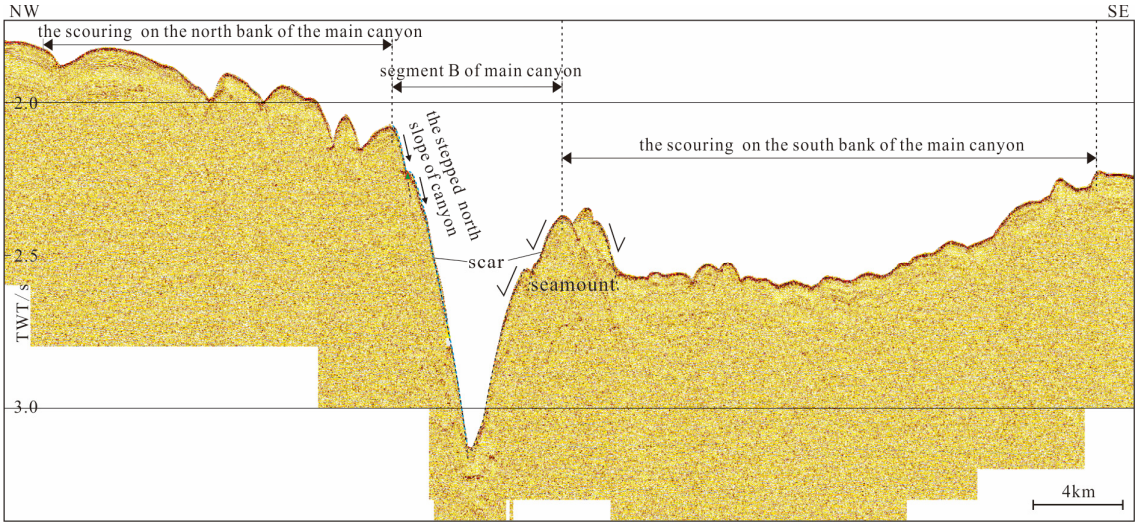


Figure 7. Seismic profile through Segment B of the main canyon (see Figure 3a for profile location).

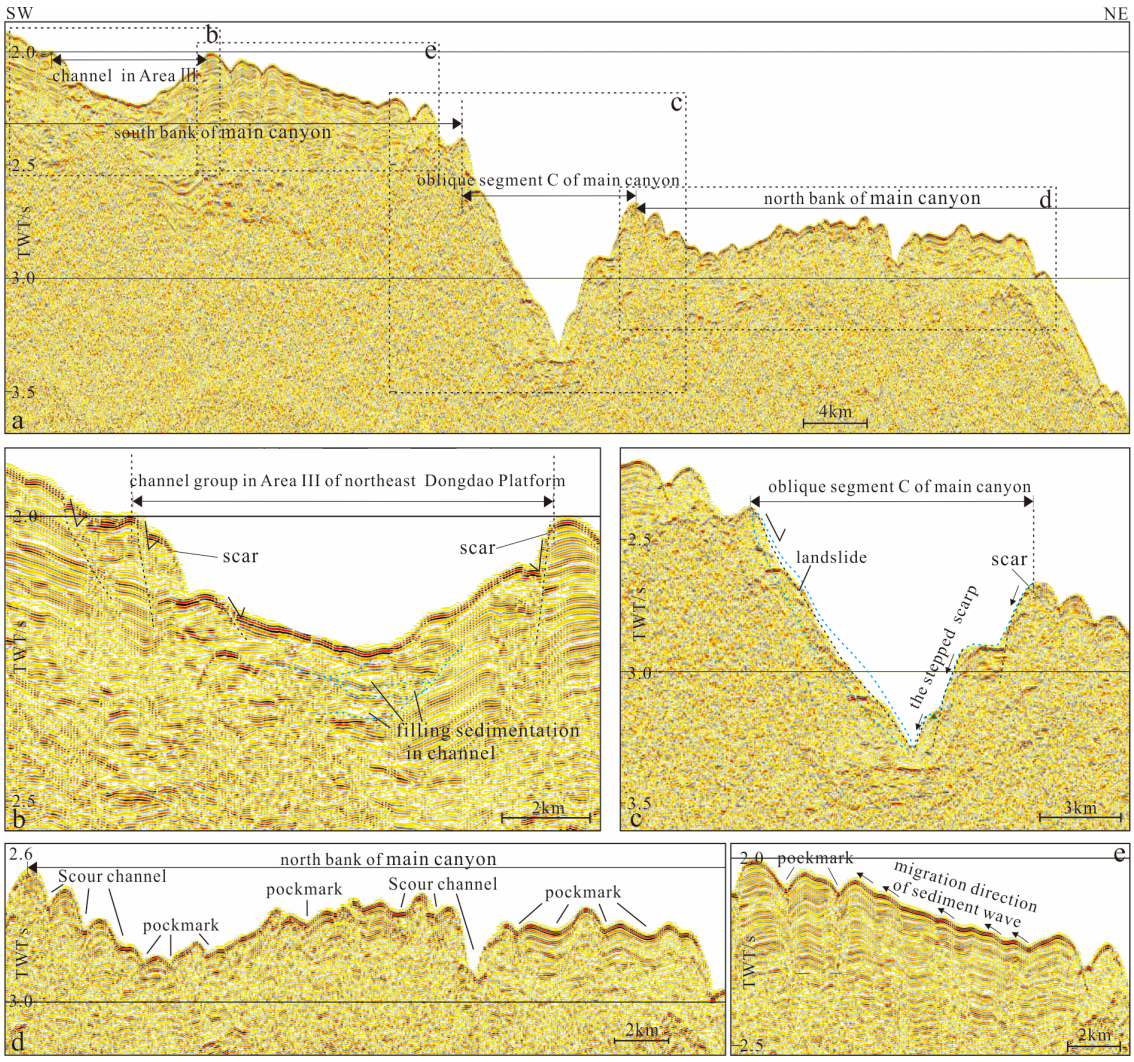


Figure 8. (**a**) Seismic profile obliquely passing through Segment C of the main canyon (see Figure 3a for profile location). (**b**) Local enlarged seismic profile (**a**), showing the details of the channel system of Area III. (**c**) Local enlarged seismic profile (**a**), showing the details of canyon Segment C. (**d**) Seismic profile on the north bank of canyon Segment C. (**e**) Seismic profile of the south bank of Canyon Segment C.

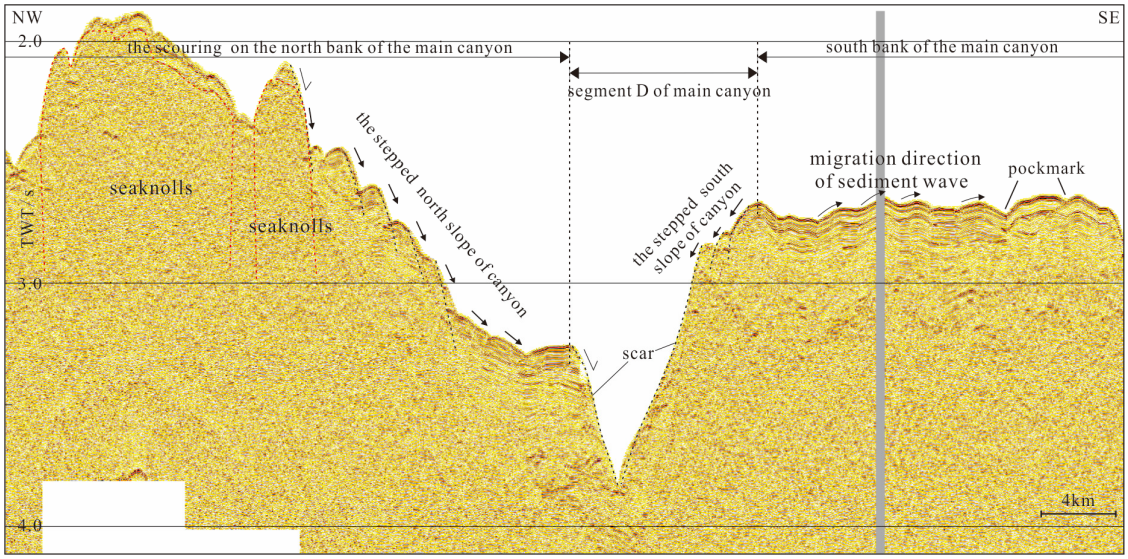


Figure 9. Seismic profile through section D of the main canyon (see Figure 3a for profile location).

4.2.3. Outside the Canyon Mouth

At the base of the continental slope (~2900 m water depth), the submarine canyons undergo pronounced widening, where sediment gravity flows are released from lateral confinement by canyon walls and spread out in a fan shape, ultimately forming channel–lobe depositional systems beyond the canyon mouth.

Vertically, the interval between the T_2 and T_1 reflectors is characterized by confined channel complexes exhibiting high-amplitude reflections and broad, U-shaped geometries. These complexes are internally filled with small-scale channels displaying disorganized configurations and low-amplitude reflection signatures. Overlying the T_2-T_1 boundary, typical channel–lobe systems are developed, which manifest sub-parallel, low-continuity reflections in cross-sectional view, forming broad, gently dipping lenticular morphologies. This vertical succession reflects a depositional transition from laterally restricted channelized facies to distributive lobe-dominated architectures (Figure 10).

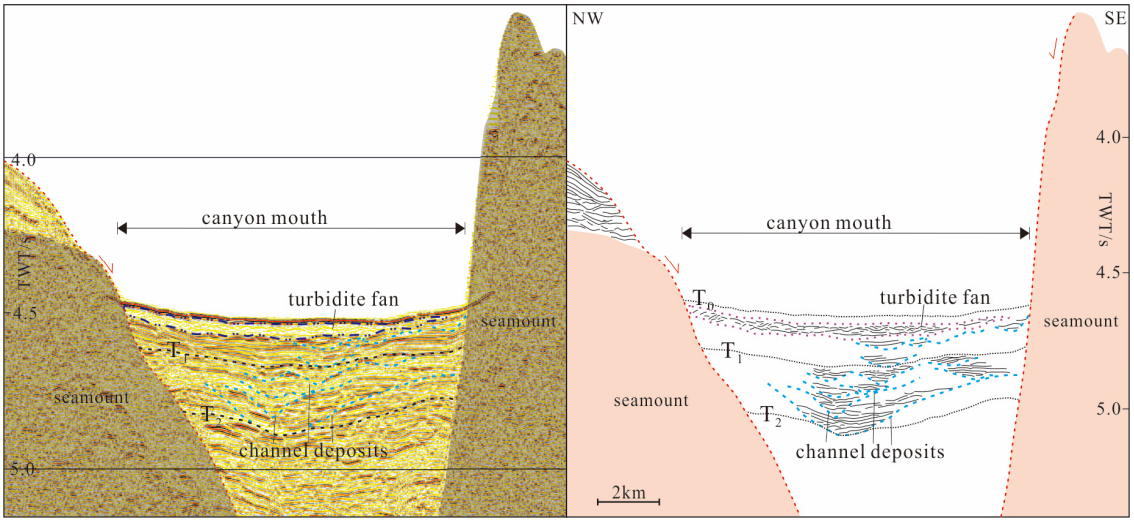


Figure 10. Seismic profile across the canyon mouth (see Figure 3a for profile location).

4.2.4. Canyon Sidewalls

The inner sidewalls of the Dongdaobei canyon are characterized by well-developed stepped scarps and extensive slumping features, reflecting ongoing slope instability. In

Segment A, the southern sidewall, located adjacent to the scouring channel group in Area III, is particularly susceptible to erosion. This erosional activity drives the retreat of the sidewall toward the channel group, resulting in the progressive widening of the canyon. The southern inner sidewall slope in this segment displays four distinct terraces separated by five scarps (Figure 6b). In contrast, the northern inner sidewall slope in Segment B exhibits a simpler morphology, with one terrace and two scarps (Figure 7). Segment C's northern inner sidewall features two terraces and three scarps (Figure 8c), while Segment D in the upper reaches of the canyon shows the most complex structure, with six terraces and seven scarps (Figure 9).

Submarine pockmarks and small channels are widely developed on the north bank of Segments A–B (Figures 6b, 8d and 9). In contrast, a small number of pockmarks developed near the bank on the southern side (Figure 8a). Another small channel developed that transported sediment and deposited it in some channels (Figure 6b) to form a scoured stepped slope in the center of the main canyon (Figures 7 and 9). The side walls of the canyon on the north bank gradually collapsed and retreated to the north and northeast as more submarine pockmarks became connected. This widened the top of the main canyon.

On the southern flank of Segments C–D, the presence of seamounts and seahills exerted significant geomorphological constraints, effectively blocking the southward extension of the channel system. Seismic profiles from Segment B revealed a distinctive depositional architecture characterized by a 250 m-thick wave-like reflection package (equivalent to 300 ms Two-Way Travel Time) beneath the canyon's southern wall. This sedimentary unit displayed the following three principal characteristics: (1) elongated parallel–subparallel configurations with continuous medium–strong amplitude reflections; (2) southeastward migration trend away from the main canyon axis; and (3) asymmetrical waveform geometry featuring steeper slope gradients on the upslope migrating flank (Figures 6b and 8a,e).

4.3. Tectonic Characteristics

During the rift stage, two predominant fault systems developed with orientations of northeast (NE) and northwest (NW). The seismic profile (traversing canyon Segment C) reveals that the canyon developed a half-graben structure controlled by pre-existing basement faults, with its axis positioned adjacent to the steeply dipping margin of the half-graben (Figure 9). Faults along the canyon sidewalls are associated with sediment instability. These small-scale faults exhibit a step-like geometry descending toward the canyon center.

Seamounts and seahills are widely distributed along the southern bank of the Dongdaobei canyon. In Area III, near the northeastern side of the Dongdao platform, a NE-trending sea ridge aligns with the platform's orientation (Figure 4a). This ridge extends nearly 10 km in length and reaches a maximum elevation of 559 m above the seafloor. In Area I, located on the northwestern side of the Dongdao platform, numerous small seamounts are observed (Figure 4a), with an average height of approximately 360 m above the seafloor. Additionally, NE-trending chains of seamounts and seahills are present along the southern bank, extending from Segment D of the main canyon to the point where the canyon enters the basin. These features rise up to 965 m above the seafloor and span a distance of 13 km.

5. Discussion

5.1. The Impact of Erosion and Deposition on Canyon Evolution

The morphological transition from V-shaped upper reaches to U-shaped lower reaches along the canyon axis reflects a systematic shift in dominant erosional and depositional processes (Figures 4 and 5). The markedly limited sediment thickness (a few tens of

meters) in the upper and middle canyon reaches, coupled with pronounced incision depths exceeding 350 m in Segments A–C, collectively indicate pervasive erosional regimes across the majority of the canyon system, while sediment thickness increases to several tens of meters in the lower reaches and near the canyon mouth, with localized accumulations reaching up to 100 m. This suggests prolonged erosional dominance since the Miocene. This evolutionary pattern is further supported by the development of turbidite fan deposits seaward of the canyon mouth, which record sustained sediment bypass during active canyon incision. It is proposed that canyon initiation is significantly influenced by slope failures and retrogressive erosion processes [35]. This interpretation is supported by the widespread occurrence of multistep terraced scarps observed along the canyon margins, accompanied by knickpoints identified in the topographic profile along the thalweg.

The sediment supply to the Dongdao canyon system is dominated by three primary mechanisms—(1) channelized transport from the western Dongdao platform (Area I) to the canyon head, (2) gravity flow deposition from the eastern platform (Area III) funneled into canyon Segment B, and (3) combined submarine landslides and channelized delivery from Area II into canyon Segment A. Particularly significant is the large-scale submarine landslide in the northwestern canyon segment proximal to Yongxing Island (Figure 3a), which spans 16 km in length with a maximum width of 15 km. This gravitational mass movement has profoundly influenced canyon evolution through dual processes. First, by introducing substantial sediment volumes directly to the canyon head and second, by inducing abrupt channel deflection through localized substrate failure and subsequent flow-path reorganization.

While these three mechanisms constitute the principal sediment sources, supplementary contributions originate from erosional gullies and small-scale landslides along the canyon flanks (Figure 6b). These secondary features intermittently deliver reworked slope sediments into the canyon system [36]. The erosional gullies and landslides, however, primarily function as supplementary supply mechanisms rather than exerting substantial influence on the canyon's overall morphological evolution.

Pockmarks serve as important indicators of the potential for slope failure and seabed instability. A large number of pockmarks are distributed around the north slope of the main canyon (Figures 4a, 6b, 8d and 9). This area is easily eroded and scoured by gravity-driven sedimentation processes and bottom currents. Continuous erosion causes the pockmarks to elongate and merge, ultimately forming immature channels. These small-scale channels are connected with the side walls of the canyon. This not only increases the sediment supply to the canyon but also widens the canyon [37,38].

5.2. The Impact of Tectonic Factors on Canyon Evolution

The formation and evolution of the Dongdaobei canyon are primarily controlled by inherited paleotopography and tectonic activities. During the Cenozoic rifting period, the region developed a graben-horst structure dominated by high-angle normal faults, which established the foundational negative topography between the Xisha carbonate platforms [5]. This inherited negative topography provided the essential geomorphological framework for the initiation of the Dongdaobei canyon. The canyon's main body consistently developed within this pre-existing negative terrain, where turbidity currents, obstructed by the surrounding seamounts and seahills, were unable to spread laterally. Instead, these currents were channeled along the slope gradient, transporting sediments to more distal areas. The steep topographic gradients on both flanks of the negative terrain further facilitated the development of gravity flows, contributing to the canyon's distinctive cross-platform orientation. Tectonic activities, particularly faulting and magmatism, played a critical role in shaping the canyon's evolution [5,39]. Two major magmatic events at

23 Ma and 10.5 Ma, along with Pliocene–Quaternary magmatic activities, significantly influenced the region's structural framework [40,41]. The NE-trending deep faults, such as those observed along the periphery of the northern canyon of Dongdao Island, align with the main extension direction of the canyon, further emphasizing the tectonic control on its development [42,43]. These faults weakened the strata, making them more susceptible to erosion and facilitating the formation of channelized features and negative topographic relief.

The directional changes and segmental evolution of the canyon are also influenced by the shielding effects of magma diapirs, seamounts, and seahills. Active magmatic bodies on both banks and the periphery of the canyon directly impact its spreading and morphology. For instance, the northeastern extension of Segment B on the north bank is obstructed by shallow seamounts with extensive base areas, forcing the canyon to turn eastward (Figure 10). Similarly, seamounts, seahills, and magmatic intrusions on the southern bank of Segment D block the canyon's extension in the eastern and southern directions, confining its development to NE and NNE trends. These topographic barriers, some reaching heights of 750 m, act as significant obstacles to the canyon's further progression, particularly as it approaches the basin. The interplay between these features and the canyon's morphology underscores the importance of local topographic controls in shaping its downstream evolution.

Sediment instability and deformation, particularly slumping, further contribute to the canyon's development. A series of SW-NE-oriented syn-sedimentary faults and associated fault scarps along the canyon's flanks promotes retrogressive failure, resulting in step-like topographic features and terraced sidewalls. These faults not only control the development of landslides on the canyon's sidewalls but also influence sediment transport pathways by obstructing pre-existing channels. The fragile depositional fault boundary zones are particularly susceptible to erosion, enhancing the incision of the canyon bottom and the widening of its cross-section. Additionally, the development of organic reefs and carbonate platforms since the Early Miocene, driven by basement uplift and the formation of peripheral horsts and fault blocks, has provided a rich source of sediment for gravity flow deposition. These carbonate deposits, transported through channels and canyons, form the basis for the canyon's sedimentary infill and geomorphological evolution.

In summary, the Dongdaobei canyon's development is a result of the interplay between erosion by sedimentary gravity flows, inherited paleotopography, tectonic activities, and local topographic barriers, which collectively govern its structural and sedimentary evolution.

5.3. Comparisons with Other Submarine Canyons of Carbonate Platforms and the Sedimentation Model

The formation factors of the Dongdaobei canyon share significant similarities with those observed in the Graham Bank region of the NW Sicily Channel (central Mediterranean Sea). Both canyons are influenced by topographic barriers, such as volcanic seamounts and fault escarpments, as well as sediment instability processes, including mass-wasting and landslides. In the Graham Bank region, the spatial distribution of volcanic seamounts, pockmarks, and fault-controlled erosive channels plays a critical role in shaping its morphological framework. Similarly, the Dongdaobei canyon's evolution is constrained by seamounts, faulting, and gravity-driven sediment transport. While the Graham Bank area exhibits distinct geological processes on its eastern (volcanic and mass-wasting dominated) and western (fluid seepage and tectonic-dominated) sides, both regions highlight the importance of tectonic and topographic controls in submarine canyon development. These parallels underscore the broader relevance of such factors in the evolution of carbonate platform-associated canyons [39].

Compared with the carbonate submarine canyons worldwide, the Dongdaobei canyon shows significant differences in scale and morphology [44]. Canyon systems supplied by pure carbonate factories hardly exceed 100 km in length. Most of these canyons are less than 50 km in length [44–46]. However, the total length of the Dongdaobei canyon actually exceeds 137 km. The formation of canyons on this scale is more favored in a siliciclastic depositional setting [3]. Submarine canyons around carbonate platforms incise along the ring-shaped margin and usually exhibit straight linear features extending downslope, which are known as line-sourced features. Sediments are transported from platform-top to adjacent deep-sea basins in the form of line-sourced supply, which will result in the development of slope aprons or base-of-slope aprons. The presence of point-sourced supply is the most crucial factor controlling the development of calciclastic submarine fans [44]. The head of Dongdaobei canyon is composed of multiple channels. Along the negative topography between the Xisha carbonate platforms, sediments from the northwest of Dongdao platform and the east of Yongxing platform coalesce downslope and form a major feeder channel (i.e., point-sourced) at the base of the ramp slope. Therefore, the calciclastic submarine fan model appears to be more reasonable than the carbonate apron models in explaining the formation and evolution process of the Dongdaobei canyon system (Figure 11).

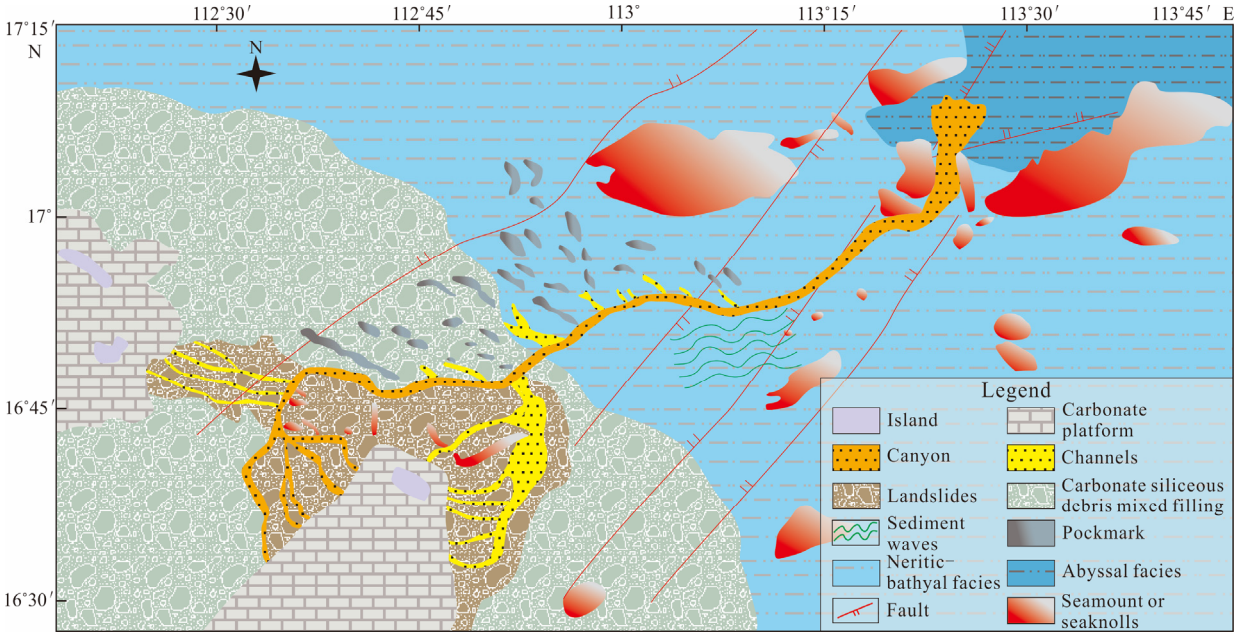


Figure 11. Schematic diagram of sedimentary facies and fault distribution around the Dongdaobei submarine canyon.

6. Conclusions

The Dongdaobei submarine canyon system in the eastern Xisha area of the South China Sea comprises a dendritic geomorphic structure, including four branched head canyons, a main canyon, and distal turbidite fans. Functioning as a critical conduit for carbonate debris transport from the Dongdao and Yongxing platforms to the Northwest Sub-basin, this system facilitates sediment delivery through diverse gravity-driven processes, such as slumping, landslides, and turbidity currents.

Sediment dynamics within the canyon are intricately linked to erosional and depositional feedback. Continuous erosion along the main canyon's northern slope has generated elongated pockmark chains, which evolve into small-scale channels connected to the canyon's sidewalls. Concurrently, seamounts distributed along the southern bank act as

topographic barriers, steering the downstream segment of the main canyon into NE-NNE orientations and restricting its lateral migration. This directional constraint underscores the role of inherited volcanic structures in shaping canyon morphology.

The evolution of the Dongdaobei canyon is ultimately governed by a combination of tectonic, topographic, and sedimentological factors. NE-trending fault systems and localized magmatic activities have weakened the strata, promoting erosion and creating preferential pathways for gravity flows. Inherited negative topography, formed during Cenozoic rifting, provided the initial framework for canyon development, while the shielding effects of seamounts and magmatic intrusions further modulated its geomorphic evolution. These interactions between tectonic forcing, sediment instability, and topographic barriers exemplify the complex mechanisms driving submarine canyon formation in carbonate platform settings.

Author Contributions: Software, X.H.; Writing—original draft, M.S.; Writing—review & editing, H.C. and C.Y.; Visualization, J.L. All authors have read and agreed to the published version of the manuscript.

Funding: The source of support for research work is the Project of China Geological Survey (No. DD20221712), as well as the China-Vietnam Joint Investigation Project on the outside and neighboring areas in the Beibu Gulf, Northern South China Sea.

Data Availability Statement: Due to privacy and other restrictions, the research data supporting the reported results cannot be shared publicly.

Conflicts of Interest: The authors declare no conflict of interest.

References

1. Normark, W.R. Growth patterns of deep-sea fans. *AAPG Bull.* **1970**, *54*, 2170–2195.
2. Popescua, I.; Lericolais, G.; Paninc, N.; Normand, A.; Dinu, C.; Drezen, E.L. The Danube submarine canyon (Black Sea): Morphology and sedimentary processes. *Mar. Geol.* **2004**, *206*, 249–265. [CrossRef]
3. Harris, P.T.; Whiteway, T. Global distribution of large submarine canyons: Geomorphic differences between active and passive continental margins. *Mar. Geol.* **2011**, *285*, 69–85. [CrossRef]
4. Xu, S.; Wang, Y.M.; Peng, X.C.; Zhuo, H.T.; Qiu, Y.; Zhou, W. Depositional Elements and Settings of HD133 and HD77 Cores in the Taiwan Canyon. *Acta Sedimentol. Sin.* **2013**, *31*, 325–330.
5. Su, M.; Zhang, C.; Xie, X.N.; Wang, Z.F.; Jiang, T.; He, Y.L.; Zhang, C.M. Controlling factors on the submarine canyon system: A case study of the Central Canyon System in the Qiongdongnan Basin, northern South China Sea. *Sci. China Earth Sci.* **2014**, *44*, 1807–1820. [CrossRef]
6. Liu, J.; Su, M.; Qiao, S.H.; Sha, Z.B.; Wu, N.Y.; Yang, R. Forming Mechanism of the Slope-confined Submarine Canyons in the Baiyun Sag, Pearl River Mouth Basin. *Acta Sedimentol. Sin.* **2016**, *34*, 940–950.
7. Posamentier, H.W.; Kolla, V. Seismic geomorphology and stratigraphy of depositional elements in deep-water settings. *J. Sediment. Res.* **2003**, *73*, 367–388. [CrossRef]
8. Pyrcz, M.J.; Catuneanu, O.; Deutsch, C.V. Stochastic surface-based modeling of turbidite lobes. *AAPG Bull.* **2005**, *89*, 177–191. [CrossRef]
9. Bernhardt, A.; Jobe, Z.R.; Lowe, D.R. Stratigraphic evolution of a submarine channel-lobe complex system in a narrow fairway within the Magallanes foreland basin, Cerro Toro Formation, southern Chile. *Mar. Pet. Geol.* **2011**, *28*, 785–806. [CrossRef]
10. McDonnell, A.; Loucks, R.G.; Galloway, W.E. Paleocene to Eocene deepwater slope canyons, western Gulf of Mexico: Further insight for the provenance of deep-water offshore Wilcox Group plays. *AAPG Bull.* **2008**, *92*, 1169–1189. [CrossRef]
11. Davies, R.J.; Thatcher, K.E.; Mathias, S.A.; Yang, J. Deepwater canyons: An escape route for methane sealed by methane hydrate. *Earth Planet. Sci. Lett.* **2012**, *323–324*, 72–78. [CrossRef]
12. Chen, H.J.; Cai, G.Q.; Luo, W.D.; Wu, J.Q.; Huang, L.; Li, L.Q. Features of Canyon Morphology and their Origin in the Shenhu area, northern Slope of the South China Sea. *Mar. Geol. Quat. Geol.* **2012**, *32*, 19–26. [CrossRef]
13. Sun, M.J.; Yao, Y.J.; Luo, W.D.; Hu, X.S.; Zhou, J.; Xu, Z.Y.; Ju, D.; Liu, J. Sedimentary Evolution Characteristics and Controlling Factors of Zhongjiannan Canyons in Northwestern South China Sea. *Earth Sci.* **2022**, *47*, 4005–4019.
14. Sun, M.J.; Gao, H.F.; Li, X.J.; Luo, W.D.; Wang, Z.; Liu, J.; Zhao, M.H. Cenozoic sequence stratigraphy and sedimentary evolution of forearc basin in Ryukyu Island Arc region. *Acta Petrol. Sin.* **2022**, *38*, 980–992.
15. Helland-Hansen, W.; Steel, R.J.; Somme, T.O. Shelf genesis revisited. *J. Sediment. Res.* **2012**, *82*, 133–148. [CrossRef]

16. Wang, X.X.; Cai, F.; Sun, Z.L.; Li, Q.; Li, A.; Sun, Y.B.; Wang, H.B.; Sun, Q.L. Tectonic and oceanographic controls on theslope-confined dendritic canyon system in the Dongsha Slope, South China Sea. *Geomorphology* **2022**, *410*, 108285. [CrossRef]
17. Li, X.J.; Wang, D.W.; Wu, S.G.; Wang, W.W.; Liu, G. Geomorphology of Sansha Canyon: I Dentification and Implication. *Mar. Geol. Quat. Geol.* **2017**, *37*, 28–36.
18. Ma, B.J.; Qin, Z.L.; Wu, S.G.; Cai, G.Q.; Li, X.B.; Wang, B.; Liu, X.Q.; Qin, Y.P. High-resolution acoustic data revealing peri-platform sedimentary characteristics in the Xisha Archipelago, South China Sea. *Interpretation* **2021**, *9*, 1–44. [CrossRef]
19. Zhou, J.; Chen, H.J.; Chen, J.L.; Yi, S.T.; Guo, L.H.; Hu, X.S.; Du, W.B.; Sun, M.J. Characteristics and distribution of geohazards since the middle Miocene of the Xisha sea area, South China Sea. *Front. Earth Sci.* **2023**, *10*, 1012144. [CrossRef]
20. Li, Z.X.; Li, X.H. Formation of the 1300-km-Wide Intracontinental Orogen and Postorogenic Magmatic Province in Mesozoic South China: A Flat-Slab Subduction Model. *Geology* **2007**, *35*, 179–182. [CrossRef]
21. Li, C.; Li, J.B.; Ding, W.W.; Franke, D. Seismic stratigraphy of the central South China Sea basin and implications for neotectonics. *J. Geophys. Res.* **2015**, *120*, 1377–1399. [CrossRef]
22. Pubellier, M.; Aurelio, M.; Sautter, B. The Life of a Marginal Basin Depicted in a Structural Map of the South China Sea. *Episodes* **2018**, *41*, 139–142. [CrossRef]
23. Li, X.J.; Wang, Z.; Yao, Y.J.; Gao, H.F.; Zhu, S.; Xu, Z.Y. The formation and evolution of the South China Sea. *Geol. Inchina* **2020**, *47*, 1310–1322.
24. Li, L.; Wang, B.; Lei, C.; Ren, J.Y.; Zhang, Y.Z.; Gao, Y.Y.; Li, L.; Liu, B.W. Tectonic Framework in the Xisha Area and Its Differential Evolution. *Earth Sci.* **2021**, *46*, 3321–3337.
25. Wu, S.G.; Zhu, W.L.; Ma, Y.S. Vicissitude of Cenozoic carbonate platforms in the South China Sea: Sedimentation in semi-closed marginal seas. *Mar. Geol. Quat. Geol.* **2018**, *38*, 1–17.
26. Zhang, G.C. Tectonic evolution of deepwater area of northern continental margin in South China Sea. *Acta Pet. Sin.* **2010**, *31*, 528–533+541.
27. Qiu, X.L.; Ye, S.Y.; Wu, S.M.; Shi, X.B.; Zhou, D.; Xia, K.Y.; Flueh, E.R. Crustal structure across the Xisha Trough, Northwestern South China Sea. *Tectonophysics* **2001**, *341*, 179–193. [CrossRef]
28. Zhu, W.L.; Xie, X.N.; Wang, Z.F.; Zhang, D.J.; Zhang, C.L.; Cao, L.C.; Shao, L. New insights on the origin of the basement of the Xisha uplift, South China Sea. *Sci. Sin.* **2017**, *47*, 1460–1468. [CrossRef]
29. Wu, S.G.; Yang, Z.; Wang, D.W.; Lü, F.L.; Lüdmann, T.; Fulthorpe, C.; Wang, B. Architecture, development and geological control of the Xisha carbonate platforms, northwestern South China Sea. *Mar. Geol.* **2014**, *350*, 71–83. [CrossRef]
30. Pang, X.; Chen, C.M.; Zhu, M.; He, M.; Liu, B.J.; Shen, J.; Lian, S.Y. Frontier of the Deep-water Deposition Study. *Geol. Rev.* **2007**, *53*, 145–151.
31. Qian, X.; Zhang, L.; Wu, S.G.; Yi, H.; Lin, Z.; Yang, Z. Sedimentary Response to Tectonic Evolution of the Northwest Sub-basin, South China Sea. *Geotecton. Metallog.* **2017**, *41*, 248–257.
32. Li, X.L.; Zhang, H.Y.; Liu, G.; Han, X.H.; Qin, Y.P.; Wu, S.G. Seismic sequence and evolution model of isolated carbonate platform—A case from Yongle Atoll, Xisha Islands. *Geol. Quat. Geol.* **2020**, *40*, 87–96.
33. Du, W.B.; Cai, G.Q.; Huang, W.K.; Chen, J.L.; Nie, X.; Wan, X.M. Seismic reflection characteristics of Neogene carbonate platforms in the Xisha Sea Area and their controlling factors. *Mar. Geol. Front.* **2021**, *37*, 20–30.
34. Zhu, W.L.; Wang, Z.F.; Mi, L.J.; Du, X.B.; Xie, X.N.; Lu, Y.C.; Zhang, D.J.; Sun, Z.P.; Liu, X.Y.; You, L. Sequence Stratigraphic Framework and Reef Growth Unit of Well Xike-1 from Xisha Islands, South China Sea. *Earth Sci. J. China Univ. Geosci.* **2015**, *40*, 677–687.
35. Hodgson, D.M.; Peakall, J.; Maier, K.L. Submarine Channel Mouth Settings: Processes, Geomorphology, and Deposits. *Front. Earth Sci.* **2022**, *10*, 790320. [CrossRef]
36. Lin, C.S.; Liu, J.Y.; Cai, S.X.; Zhang, Y.M.; Lv, M.; Li, J. Sedimentary composition and development background of large incised valley and submarine gravity flow system in Yinggehai-Qiongdongnan Basin. *Chin. Sci. Bull.* **2001**, *46*, 69–72. [CrossRef]
37. Hovland, M.; Gardner, J.V.; Judd, A.G. The significance of pockmarks to understanding fluid flow processes and geohazards. *Geofluids* **2002**, *2*, 127–136. [CrossRef]
38. Huang, Y.; Cheng, J.; Wang, M.; Wang, S.; Yan, W. Gas Hydrate Dissociation Events During LGM and Their Potential Trigger of Submarine Landslides: Foraminifera and Geochemical Records from TwoCores in the Northern South China Sea. *Front. Earth Sci.* **2022**, *10*, 876913. [CrossRef]
39. Spatola, D.; Micallef, A.; Sulli, A.; Basilone, L.; Ferreri, R.; Basilone, G.; Bonanno, A.; Pulizzi, M.; Mangano, S. The Graham Bank (Sicily Channel, central Mediterranean Sea): Seafloor signatures of volcanic and tectonic controls. *Geomorphology* **2018**, *318*, 375–389. [CrossRef]
40. Ma, Y.; Wu, S.G.; Lv, F.L.; Dong, D.D.; Sun, Q.L.; Lu, Y.T.; Gu, M.F. Seismic characteristics and development of the Xisha carbonate platforms, northern margin of the South China Sea. *J. Asian Earth Sci.* **2011**, *40*, 770–783.
41. Feng, Y.C.; Zhan, W.H.; Sun, J.; Yao, Y.T.; Guo, L.; Chen, M. The formation mechanism and characteristics of volcanoes in the Xisha waters since Pliocene. *J. Trop. Oceanogr.* **2017**, *36*, 73–79.

42. Zhong, G.J.; Feng, C.M.; Wei, Z.Q. The Structural Features of Xisha Trough Basin. *Mar. Geol. Quat. Geol.* **2012**, *32*, 63–68. [CrossRef]
43. Briais, A.; Patriat, P.; Tapponnier, P. Updated Interpretation of Magnetic Anomalies and Seafloor Spreading Stages in the South China Sea: Implications for the Tertiary Tectonics of Southeast Asia. *J. Geo Phys. Res. Solid. Earth* **1993**, *98*, 6299–6328. [CrossRef]
44. Payros, A.; Pujalte, V. Calciclastic submarine fans: An integrated overview. *Earth-Sci. Rev.* **2008**, *86*, 203–246. [CrossRef]
45. Chen, J.J.; Wu, S.G.; Li, Q.; Wei, C.L.; Fu, G.W.; Chen, W.L.; Qin, Y.P.; Khan, U.; Wu, S.L. Morphology and evolution of submarine canyons around the Zhongsha Platform, South China Sea: Implications for sedimentary processes in a modern isolated carbonate setting. *Mar. Geol.* **2024**, *475*, 107362. [CrossRef]
46. Li, S.; Alves, T.M.; Li, W.; Wang, X.J.; Rebesco, M.; Li, J.; Zhao, F.; Yu, K.Q.; Wu, S.G. Morphology and evolution of submarine canyons on the north west South China Seamargin. *Mar. Geol.* **2022**, *443*, 106695. [CrossRef]

Disclaimer/Publisher's Note: The statements, opinions and data contained in all publications are solely those of the individual author(s) and contributor(s) and not of MDPI and/or the editor(s). MDPI and/or the editor(s) disclaim responsibility for any injury to people or property resulting from any ideas, methods, instructions or products referred to in the content.